SYNTHESIS AND CHARACTERIZATION OF HYDROXYAPATITE POWDER FROM CATTLE BONE

Agbeboh Newton Itua[1,2], Oladele Isiaka Oluwole[1,3], Sanjay Mavinkere Rangappa[4], Suchart Siengchin[4]

[1]*Department of Metallurgical and Materials Engineering*
Federal University of Technology
Akure, Ondo State, Nigeria
[2]*Department of Mechanical and Mechatronics Engineering*
Federal University Otuoke
P.M.B. 126, Yenagoa, Bayelsa State, Nigeria
[3]*Centre for Nanomechanics and Tribocorrosion*
School of Metallurgy, Chemical and Mining Engineering
University of Johannesburg
Johannesburg, South Africa
[4]*Natural Composites Research Group Lab*
Department of Materials and Production Engineering
The Sirindhorn International Thai-German Graduate School of Engineering
(TGGS), King Mongkut's University of Technology North Bangkok
Bangkok (KMUTNB), Thailand
E-mail: newtoncitua@yahoo.com

Received 18 October 2022
Accepted 20 March 2023

ABSTRACT

In this research the possibility of synthesizing hydroxyapatite powder (HAp) from cattle (cow) bone was investigated. Cattle bone (CB) was processed using two different variants of wet chemical precipitation methods. Two sets of samples were produced from the method that was based on the use of analytical grade concentrated orthophosphoric acid (H_3PO_4) while the other one was based on nitric acid (HNO_3) in combination with diammonium hydrogen phosphate ($(NH_4)_2HPO_4$). The developed HAps were characterized with XRD to ascertain the sample with optimum HAp yield. It was discovered from the results that high purity HAp was achieved from calcined bone without any chemical precipitation. Thus, functional groups, morphology and particle size were determined using Fourier Transform Infrared Spectroscopy (FTIR), RAMAN and SEM analyses for the calcined cow bone. The results showed that, pure HAp can be obtained in calcined cow bone without chemical synthesis. The research revealed the possibility of obtaining high quality HAp from non-synthetic source with low technological processes that are more environmentally and economically friendly.

Keywords: cattle bone, hydroxyapatite, chemical synthesis, non-synthetic, environmentally friendly.

INTRODUCTION

Implant usage has become a common means of improving the living conditions of people with a variety of hard tissue problems arising from disease, aging and accidents. The human body is made up of a complex network of bones, teeth and other hard tissues called the skeletal system. This interconnected network of hard tissues form a frame responsible for the rigid upright posture of the human being. Bones are composed of two major layers the cancellous and the cortical layers. Teeth are made up of enamel and dentin which is the strongest material in the skeletal system of the human body. It is used for cutting, biting, mastication and chewing of food. The adult human has a total of about 32 teeth and 206 bones which are made up of different organic and inorganic materials. The organic constituents consist of approximately 90 % of a type of triple-helical molecule

made up of amino acids, known as collagen type I and about 10 % noncollagenous proteins [1, 2].

The inorganic constituents consist of minerals containing mostly calcium and phosphates in an apatite lattice. The most common of which is hydroxyapatite HAp with a CaP ratio of 1.67 [3]. The cortical and cancellous layers of bones contain about 60 % HAp while the foundation of tooth enamel contains about 90 % HAp [4]. Phase pure HAp consist of 39.68 wt. % calcium and 18 wt. % phosphorus resulting in a 1.67 mole ratio of Ca/P.

In reality, the Ca/P ratio of commercial HAp products may be smaller than 1.67 or bigger. The phase shift is indicated by the Ca/P ratio which specifically varies between tricalcium phosphate (TCP) and calcium oxide (CaO). HAp with a Ca/P ratio above 1.67 is made up of more CaO than TCP while HAp with a Ca/P ratio below 1.67 is composed of more TCP than CaO [5].

HAp is one of the most biocompatible and bioactive calcium phosphate materials as it possesses a mineral phase close to that of bone. It is usually used as a protective coating on implant materials, or as a reinforcement to facilitate implant incorporation and trigger bone regrowth. Synthetic HAp is quite expensive and as such there is the need for research into alternate sources of phase pure stoichiometric HAp [6]. Green sources are some of the most promising sources of HAp which consists of plant, animal and mineral. These sources have the advantage of being cheaper, environmentally friendly, recyclable, possibility of regeneration or regrowth over time and likely reduction of material depletion. However, there is the need to improve on the quality and quantity of HAp yield by improving and enhancing the production processes which has been the focus of recent researches. Despite this, there has not been clear comparison of the yield the various wet chemical precipitation processes. This work was therefore, carried out to investigate comparatively the influence of orthophosphoric acid and nitric acid, respectively, on the yield of HAp from cow bone in terms of phase purity and quantity.

EXPERIMENTAL

Materials

The materials used for this study are cow bones obtained from an abattoir located at latitude 7°17'01.3"N and longitude 5°11'15.8"E in Akure, Ondo State, Diammonium hydrogen phosphate, nitric acid, orthophosphoric acid and ammonium hydroxide obtained from Pascal Chemicals Akure.

Procurement and processing of the cow bones

The cow bones were gathered together and cleaned to remove all the debris, sand and other impurities, after which they were washed using distilled water and sun-dried within 5 days. The materials were then sorted into batches, and boiled separately to remove the leftover organic materials and membranes, after which they were washed again, cleaned, and dried in an oven at 80°C for 24 hours. The dried materials were weighed and put into sizeable ceramic crucibles and then charged into a muffle furnace. This was done to convert the materials to calcium oxide via a three-stage calcination process outlined in Table 1 in accordance with Agbabiaka et al., 2020 [7].

After calcination, the samples were allowed to cool to room temperature within the furnace and the

Table 1. Three Stage Calcination Temperature Chart.

Stage No.	Temp. Range, ^oC	Heating Rate, $^oC\ min^{-1}$	Final Temp., ^oC	Soaking Time, hrs	Effects Observed
1	25 - 450	12	450	1	Smoke indicating the burning off of the membranes and organic materials
2	450 - 700	8	700	2	Decarbonisation, CO_2 emission, organic compounds and protein burn off
3	700 - 1000	4	1000	3	Complete decarbonisation and transformation into calcium oxide CaO and calcium hydroxide $Ca(OH)_2$

resulting whitish solid products were mechanically crushed with a laboratory jaw crusher followed by pulverizing to smooth powdery form using a laboratory ball mill operated at 300 rpm. The fine granular material produced composed mainly of calcium carbonate was sieved using a sieve with 90 μm aperture size to obtain powders with the required particle size of less than 90 μm. The calcined cow bone powders were divided into two sets of 500 g each for use as starting materials to derive hydroxyapatite via the two different wet chemical precipitation processes. Hydroxyapatite powders were synthesised using the chemical reagents: diammonium hydrogen phosphate ($(NH_4)_2HPO_4$), nitric acid (HNO_3) of 99 % purity, ammonium hydroxide ($(NH_4)OH$), and analytical grade 99 % pure orthophosphoric acid (H_3PO_4).

Hydroxyapatite synthesis using orthophosphoric acid

To carry out the synthesis, 5 g each of CaO was measured into three separate beakers each containing 100 mL of distilled water and were subjected one after the other to the same orthophosphoric acid based wet chemical precipitation process. Each beaker containing the solution was placed on a hot plate magnetic stirrer and allowed to boil while the solution was thoroughly stirred. The stirring was carried out continuously for 3 hours and as the solution boiled, an effervescent reaction was observed, signifying that CaO was being transformed to $Ca(OH)_2$ in accordance with the observation made by Bonou et al. [8]. The reaction proceeded according to the chemical equation stated in Eq. (1):

$$10CaO + 10H_2O \rightarrow 10Ca(OH)_2 \quad (1)$$

The solution was then reacted with 20 mL of 99 % purity analytical grade orthophosphoric acid (H_3PO_4) while stirring at 120 rpm according to the processes outlined by Hui et al. [9]. A suspension of precipitates was initially observed, which dissolved upon further stirring for about 30 minutes after which the precipitates were completely dissolved into the solution. After all the precipitates had dissolved, indicating the completion of the reaction, stirring was stopped and the beaker was removed from the heating medium while allowed to cool and age for 7 days according to the processes outlined by Oladele et al. [10]. Eq. (2) showed the chemical equation for the reaction.

$$10Ca(OH)_2 + 6H_3PO_4 \rightarrow Ca_{10}(PO_4)_6(OH)_2 + 18H_2O \quad (2)$$

After aging, the solution was filtered using filter paper and the residue was oven-dried at 105°C for 1 hour. The dried residue was then put in a crucible and transferred to a furnace where it was subjected to heat-treatment in three stages. Table 2 summarises this process of heat treatment that caused the HAp to crystallize and undergo sintering to form dendrites which agglomerated into lumps. The samples were allowed to cool in the furnace and thereafter removed. The lump

Table 2. High Temperature Sintering chart for the HAp powders derived using orthophosphoric acid.

Stage No.	Temp. Range, ^oC	Heating Rate, $^oC\ min^{-1}$	Final Temp., o*C*	Soaking Time, hrs	Effects Observed
1	25 - 425	5	425	0	Boiling of the chemicals and slight smoking as the fumes from the chemicals evaporate and due to emission of gases, gradual transformation to solution as the temperature increases.
2	425 - 700	10	700	0	Slight boiling and fume emission due to the release of gases upon heating, leaving a slightly agglomerated, red hot, gelatinous substance.
3	700 - 1000	15	1000	3	Total liquefaction of sample and upon cooling the sample is transformed to hard sintered whitish solid.

formed was then pulverized using a laboratory jaw crusher and milled to powder using a ball mill with steel balls. The powdered particles were then subjected to sieve analysis after grinding to determine the particle size, and particles of 90 μm sieve aperture passing were obtained.

The full chemical reaction of the complete process is adjusted in Eq. (3) to show the reaction between CaO and water to form calcium hydroxide, and the precipitation of hydroxyapatite upon reaction with orthophosphoric acid:

$$10CaO + 10H_2O + 6H_3PO_4 \rightarrow Ca_{10}(PO_4)_6(OH)_2 + 18H_2O \quad (3)$$

Eq. (3) is, therefore, the expected chemical equation for the synthesis of hydroxyapatite using orthophosphoric acid-based wet chemical precipitation method.

Hydroxyapatite synthesis using diammonium hydrogen phosphate and nitric acid

The same procedure above was followed using nitric acid of 99 % purity and diammonium hydrogen phosphate salt in stoichiometric amounts according to the steps outlined by Rujitanapanich et al. [11]. This was carried out by first measuring 3 g each of CaO into beakers and successively reacting with 25 % nitric acid while stirring constantly using a magnetic stirrer at room temperature for 2 hours to obtain calcium nitrate $Ca(NO_3)_2$. After the heat emitting reaction, the solution was allowed to cool down to room temperature and 12.73 g of diammonium hydrogen phosphate ($(NH_4)_2HPO_4$) dissolved in 30 mL distilled water was added drop wise to the solution. The formation of precipitates was observed with each drop of diammonium hydrogen phosphate (DAHP). The pH was monitored using a pH meter, and maintained between 8 - 10 using ammonium hydroxide ($(NH_4)OH$). Throughout the reaction, the solution was constantly stirred and precipitates formed rapidly. A homogenous reaction was maintained which occurred according to the processes outlined by Akram et al. [12] with the chemical Eqs. (4) and (5):

$$CaO + 2HNO_3 \rightarrow Ca(NO_3)_2 + H_2O \quad (4)$$

$$10Ca(NO_3)_2 + 6(NH_4)_2HPO_4 + 8NH_4OH \rightarrow \rightarrow Ca_{10}(PO_4)_6(OH)_2 + 20NH_4NO_3 + 6H_2O \quad (5)$$

Upon completion of the reaction the solution was allowed to age for 24 hours and then washed with distilled water to obtain clear white precipitates. The precipitates were then filtered using a filter paper and oven-dried at 120°C for 3 hours. The dried precipitates were then transferred into a ceramic crucible and calcined in an electric muffle furnace via a two stage calcination process summarised in Table 3. The powdered particles were then allowed to cool in the furnace and thereafter removed, milled and sieved to obtain less than 90 μm sieve passing.

Characterization and testing

SEM/EDS Analysis

Scanning Electron Microscopy (SEM) using a Carl Zeiss Sigma Field Emission Gun Scanning Electron Microscope, with Energy Dispersive Spectrometer (EDS), was utilized in examining the surface of the dried sample powders and determining the extent of particle agglomeration, its morphology and microstructure.

Table 3. High Temperature Sintering chart for the Hydroxyapatite powders Synthesised using Diammonium Hydrogen Phosphate and Nitric Acid.

Stage No.	Temp. Range, ^oC	Heating Rate, $^oC\ min^{-1}$	Final Temp., ^oC	Soaking Time, h*rs*	Effects Observed
1	25 - 700	10	700	1	Boiling of the chemicals (including trace amounts of water) and slight smoking as the water vapour, gases and fumes from the chemicals evaporate leaving a white solid powder as dendrites are formed and crystallization begins.
2	700 - 1000	15	1000	3	Agglomeration of the crystals into flake like white solid structures.

XRD Analysis

X-Ray Diffraction (XRD) analysis was performed using a Bruker D2-phaser X-Ray Diffraction machine with Cu Kα radiation (λ = 0.154060 nm), with a scan step of 2° min^{-1} in the 2θ range of 5° to 90°, to characterize and study the diffraction patterns of the sample powders and their phase composition.

Fourier Transform Infrared Spectroscopy (FTIR) Analyses

An FT-IR spectrometer (Infrared spectrometer Bruker Vertex 70 Hyperion 1000 FTIR Spectrometer with diamond Attenuated Total Reflectance (ATR) accessories was used to confirm the chemical structure of all samples and obtain information about the functional groups of the prepared HAp powders.

Raman Microspectroscopy

A laser Raman micro-spectrometer (inVia™ confocal Raman microscope from Renishaw) was used to characterize the synthesised HAp powders. Each sample was exposed to a green laser (532 nm wavelength) for a period of 5 s at a laser power density of 1 × 105 W cm^{-2}. Raman spectra for wavenumbers within ~2670 cm^{-1} - 110 cm^{-1} were acquired with a 600 g mm^{-1} grating (spectral resolution of ~4 cm^{-1}). A × 100 objective lens (NA = 0.9) was used to achieve Raman analysis spatial resolution of < 1 µm, and the incident laser power was estimated to be ~0.4 m.W at the sample surface.

RESULTS AND DISCUSSION

X-Ray diffraction

Compositional and structural characterization was carried out to determine the internal crystal structure and composition of the hydroxyapatites. The initial qualitative and quantitative compositional analyses of the different samples were performed using XRD. The XRD patterns of the pulverized and calcined cow bones were analysed, with each individual spectrum developed via a plot of intensity (counts) as a function of position *2θ*, and then the resulting spectra are presented in Figs. 1 - 3. The peaks were compared and matched with the Powder Diffraction File (PDF) from the database of the Joint Committee on Powder Diffraction Standards - the International Centre of Diffraction Data (JCPDS-ICDD) and the Inorganic Crystal Structure Database (ICSD). From the results and the spectrum shown on Fig. 1, it was observed that the calcined cow bone powders contained majorly stoichiometric Hydroxyapatite ($Ca_{10}(PO_4)_6(OH)_2$) with major characteristic peaks at *2θ* positions 11.16°, 32.07°, and 46.97°, Portlandite ($Ca(OH)_2$) with minor peaks at *2θ* positions 34.35° and 50.76°, and Lime (CaO) with a minor peak at *2θ* position 32.49°. Each sample was also found to contain trace amounts of other compounds, attributed to inorganic elements from the debris including silica left on the flesh after washing, residual carbon from the calcination process and iron from the metal ball mills used in pulverizing the bones.

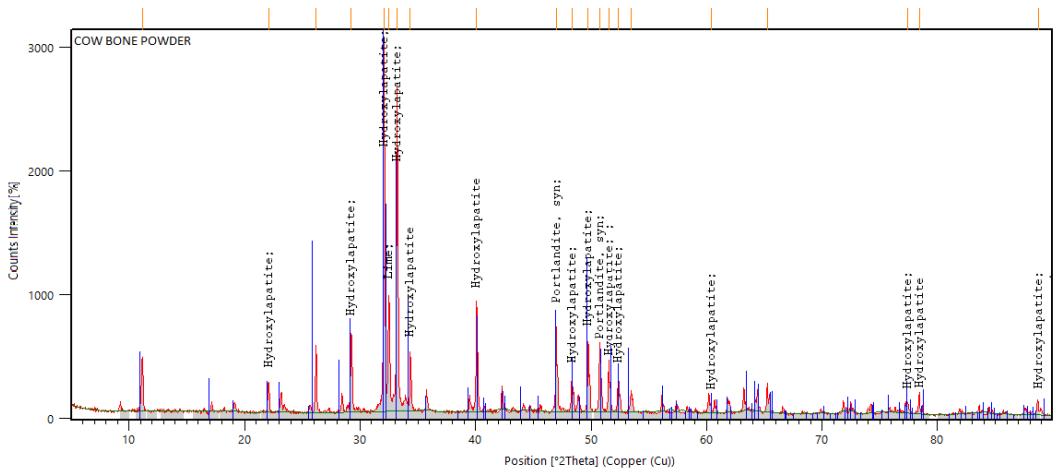

Fig. 1. XRD pattern of the calcined cow bones.

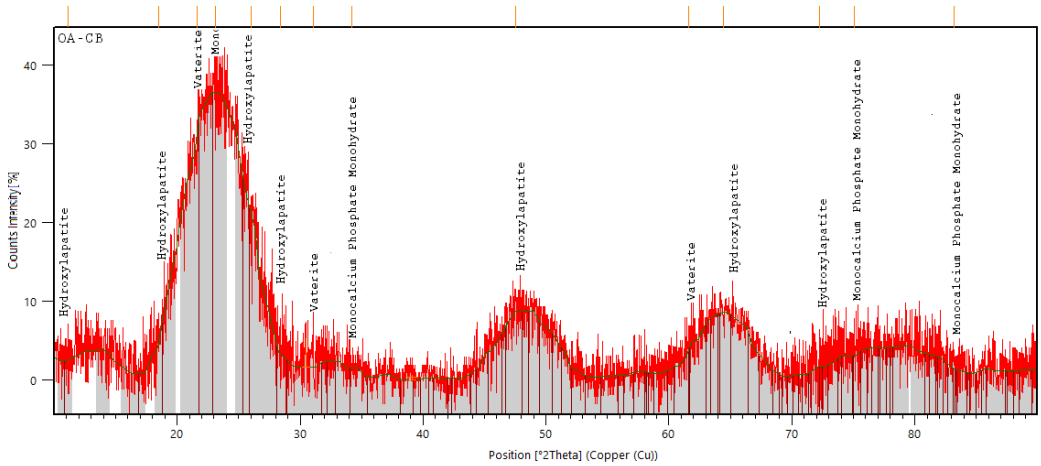

Fig. 2. XRD pattern of orthophosphoric acid based wet chemical precipitated cow bones.

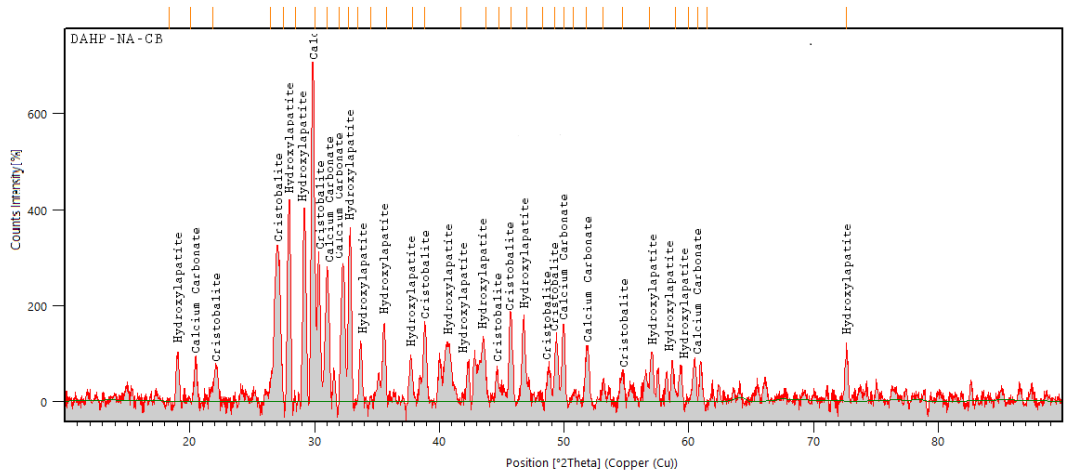

Fig. 3. XRD pattern of diammonium hydrogen phosphate and nitric acid based wet chemical precipitated cow bones (DAHP-NA-CB)

The relative composition by weight percent of each of the major phases within the cow bone samples were shown in Table 4. The data were calculated from the integrated characteristic peak intensities at different 2θ positions after normalizing using the standard integrated peak intensities of each major phase. It was evident that upon calcination, cow bones contain mainly hydroxyapatite phases even without the use of additional processing methods [12, 13].

The presence of other calcium phosphate phases with different Ca/P ratios and crystallographic parameters in the samples as shown in Table 4, indicate the incomplete transformation of the reaction constituents in both wet chemical precipitation methods. This could be as a result of insufficient reaction and aging time, since phase changes occur at different periods in the reaction [14].

The variance in calcium phosphate phases is most pronounced in Orthophosphoric Acid Based Wet Chemical Precipitation Method (OAB-WCP), because the calcium carbonate phases dissolve rapidly as soon as the orthophosphoric acid is added. A sharp change in pH is observed, induced by the dissolution of acidic carbonates, and the precipitation of brushite phases as carbon dioxide gas is released [15]. Upon the continuous dropwise addition of the orthophosphoric acid, the reaction progresses and the newly precipitated brushite

Table 4. XRD Quantification of the Calcium Phosphate Composition of Samples (wt.%).

Sample	Hydroxyapatite ($Ca_{10}(PO_4)_6(OH)_2$)	Lime (CaO)	Portlandite (Ca(OH)2)	Calcite ($CaCO_3$)	Other Phases
CB	80	6	3	1	10
OA-CB	60	2	4	3	31
DAHP-NA-CB	77	1	1	0	21

OA-CB: Orthophosphoric acid treated cow bones; DAHP-NA-CB: Diammonium Hydrogen Phosphate and Nitric acid treated cow bones.

phases are again dissolved while a more stable monetite phase is precipitated. A gradual decrease of carbonates and an increase in pH was observed, as aragonite phases were dissolved while more monetite phases were formed [16]. As calcite, brushite, and aragonite phases were rapidly dissolved, a dissolution-reprecipitation chain reaction was observed which continued till a more thermodynamically stable system was precipitated. This rapid chain reaction is believed to have influenced the structure of the resultant crystals [8, 17].

On the other hand, the diffraction pattern of OA-CB shown in Fig. 2, illustrates that the OAB-WCP to a large extent hydrates the calcium compounds within the cow bones, forming an amorphous solid made up 60 % hydroxyapatite, 1 % lime, 2 % portlandite, 37 % of calcium phosphate, octacalcium phosphate and hydrogen phosphite compounds. This signifies that there is an increase in the volume of hydrogen and phosphorus reacting with the calcium in the initial hydroxyapatite compounds due to the addition of the H_3PO_4 (orthophosphoric acid) and H_2O (water), which contributes to the formation of various amorphous hydrogen phosphate and calcium phosphates compounds. The amorphous nature of the materials resulted in a spectra in which the major peak was large and drawn out between the $2\theta 2\theta$ positions of 18° and 29° with minor sharp peaks at 23.4°, 25.8°, 31.7°, 32.4°, 49.5° and 50.4°. These signify the presence of hydroxyapatite, monocalcium phosphate monohydrate and vaterite peaks respectively similar to reports by Gergely et al. and Oladele et al. [18, 19].

Conversely, the Diammonium Hydrogen Phosphate and Nitric Acid Based Wet Chemical Precipitation Method (DAHP-NAB-WCP), precipitated both HAp and other carbonated apatites as soon as the diammonium hydrogen phosphate (DAHP) salt was added dropwise to the solution. A change in pH was observed as a result of the addition of the alkaline medium and this facilitated the synthesis of a stable hydroxyapatite phase [20]. During this reaction, several lacunae were created at the hydroxide and/or calcium sites resulting in an affinity of apatite phases to other ionic species which led to the precipitation of carbonated apatites apart from stoichiometric hydroxyapatite [8]. These other apatite structures were further crystallized as phosphate ions were replaced by carbonate ion and integrated into the apatite structures, developing into apatite phases like α-TCP and β-TCP [21]. The details of all the calcium phosphate phases precipitated using both wet chemical precipitation methods and their different compositions are shown Table 4.

From the compositional analysis of the diffraction pattern of cow bone labelled DAHP-NA-CB shown in Fig. 3 which was treated using the DAHP-NAB-WCP, it was observed that the sample yielded improved hydroxyapatite of over 77 wt. % and approximately 22 wt. % other calcium phosphate compounds and phases with trace amounts of silicon oxide. The spectra exhibited major characteristic peaks at *2θ* positions 28.13°, 32.8°, 35.5° and 49.5° and suggests the formation of a high purity hexagonal hydroxyapatite phase [22]. High intensity peaks were also observed at *2θ* positions 20.4°, 24.4°, 30°, 36°, and 45.6° for monoclinic calcium carbonate with the peak at a *2θ* position of 30° exhibiting the highest intensity on the spectra. Silicon oxide peaks were also observed, indicating the presence of a cristobalite phase with an intense peak observed at *2θ* position 22°, possibly due to the presence of silicon based impurities within the cow bone powders.

The analysis revealed that, untreated CB powder contains hydroxyapatite compounds with a Ca/P ratio of 1.67 and a few other calcium phosphate compounds with

varying Ca/P ratios while the Ca/P ratios for OA-CB and DAHP-NA-CB are 1.63 and 1.58, respectively. Hence, compared to human bone, CB possessed the closest value and was selected for further analysis. The two wet chemical precipitation methods have significantly increased the amount of calcium deficient or substituted compounds in the form of monocalcium, dicalcium, tricalcium, octacalcium and untransformed calcium phosphates with varying Ca/P ratios. It is therefore, evident from the results that the use of both wet chemical precipitation methods on the cow bone powders reduces the purity and negatively affects the quality of the hydroxyapatite content. Based on the XRD results that reveal CB as the best sample in terms of HAp yield and quality, FTIR, RAMAN and SEM analyses were further carried out on the CB sample.

Fourier transformed infrared spectroscopy (FT-IR)

The chemical constituents and functional groups of advisable the selected hydroxyapatite samples were analysed using FT-IR to avoid any ambiguous conclusions and further corroborate the XRD results, the wave numbers and absorption refractogram obtained from FT-IR spectroscopy were tabulated in Table 5 and several bands which depict the hydroxyapatite spectrum are shown in Fig. 4. The FT-IR spectrum of the sample with the highest hydroxyapatite yield, which consists of untreated cow bones after calcination designated as CB, is shown in Fig. 4. Different vibration bands were observed which showed all the characteristic absorption peaks of biological hydroxyapatite. The most characteristic chemical groups observed within the spectrum were PO_4^{2-}, PO_4^{3-}, OH^- and CO_3^{2-}. Normally natural or biological hydroxyapatite is calcium deficient and non-stoichiometric (exhibiting a Ca/P ratio higher than 1.67), it is substituted with a carbonate and as such contains carbonate groups, also some Mg and other ions are usually built into its structure [23]. There are commonly, two types of carbonate substitutions possible and biological apatites undergo both types: the first being direct substitution of OH- with CO_3^{2-} (A-type substitution $(CO_3)^{2-} \leftrightarrow 2OH^-$) and the second being indirect substitution in which carbonate CO_3^{2-} ions occupy the sites (B-type substitution). The band at 800.73 cm^{-1} is due to C-O-C symmetric stretching indicative of the ratio of carbonaceous matter remaining within the chemical structure of the material [24]. This is further buttressed by the band at 798.41 cm^{-1} which

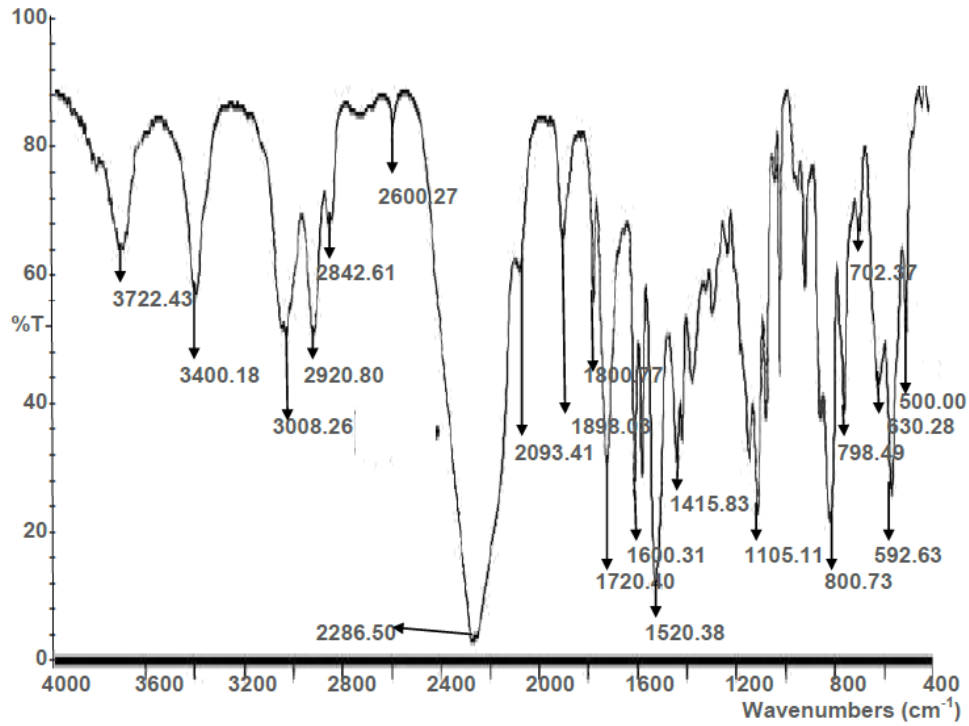

Fig. 4. FT-IR spectrum of untreated calcined cow bones.

Table 5. FT-IR spectroscopy wave number and absorption refractogram for sample C (untreated cow bone sample).

Run #	Peak, cm^{-1}	Transmittance, %	Absorbance	Assignment
1	3722.43	65.18	0.1859	O-H Stretching vibratio*n*
2	3400.18	56.93	0.2447	N-H Stretching
3	3008.26	52.71	0.2781	-C=C- stretching
4	2920.80	52.58	0.2792	symmetric stretching- vibration of the aliphatic -CH_2 group
5	2842.61	68.09	0.1669	C-H stretching of - CH_2
6	2600.27	85.71	0.0670	C=N stretching
7	2286.50	4.62	1.3354	O=C=O Stretch*ing*
8	2093.41	60.51	0.2182	C=O stretching
9	1898.03	68.72	0.1629	C=N stretch*ing*
10	1800.77	57.10	0.2434	O-H bending vibrati*on*
11	1720.40	32.61	0.4867	-C-O stretching
12	1600.31	24.10	0.6180	CH2 asymmetric variation
13	1415.33	36.21	0.4412	deformation CH2 + C=C of the aromatic r*ing*
14	1105.11	32.36	0.4900	PO_4 stretching vibration
1*5*	800.73	24.22	0.6158	C-O-C symmetric stretching
16	798.41	40.13	0.3965	C=C aromatic stretching
17	702.37	72.46	0.1399	Heteroatom vibration frequency of sulphur and nitrogen
18	630.28	43.21	0.3644	O-H stretching
19	592.63	28.23	0.5493	PO_4^{3}- stretching vibration
20	500.00	57.11	0.2435	PO_4 stretching vibration

is due to C=C aromatic stretching and is very close to the characteristic vibration band at 792.77 cm^{-1} which is attributed to O-Si-O stretching and bending vibrations [25]. The high intensity band at 1105.11 cm^{-1} is associated with a ($v3$) PO_4 monetite phase which indicates the presence of dicalcium phosphate anhydrous. However the low intensity characteristic vibration band at 702.37 cm^{-1} is due to the heteroatom vibration frequency of sulphur and nitrogen confirming the presence of sulphur and nitrogen ions within the cow bone sample. Structural O-H groups were observed at 630.28 cm^{-1} which further signifies the possibility of moisture being absorbed from the atmosphere and the occurrence of direct substitution of OH- with CO_3^{2-} which is an A-type substitution ($(CO_3)^{2-} \leftrightarrow 2OH^-$). A sharp PO_4^{3-} stretching vibration band was also observed at 592.63 cm^{-1} which indicates the presence of phosphates in the ($v3$) PO_4 mode of hydroxyapatite. The characteristic vibration band observed at 500.00 cm^{-1} corresponds to ($v4$) PO_4 brushite [26]. This shows that the various vibration bands observed in this sample confirms the presence of natural non-stoichiometric hydroxyapatite and other biological apatites and ions within the calcined cow bone sample.

Raman spectroscopy was carried out on this same sample for further confirmation and corroboration of the results.

Raman spectroscopy

The exceptional signal to noise ratio of hydroxyapatite indicates that it is an intense Raman scatterer. The values obtained from the typical Raman spectral data of hydroxyapatite synthesised from CB, were analysed. The Raman spectrum of calcined cow bone is shown in Fig. 5. Major sharp peaks were observed at 962.76, 1123.53, 2103.70, 2126.38, and 3078.10 cm^{-1}. The peaks at 429.21 and 591.72 cm^{-1} corresponds to the O−P−O bending modes ($v2$) of the PO_4^{3-} group [27]. The peak at 961.15 cm^{-1} signifies the ($v1$) totally symmetric stretching mode of the tetrahedral PO_4 group (P−O bond). The peak at 1047.50 cm^{-1} indicates the presence of a ($v3$) triply degenerate asymmetric stretching mode of the phosphate group (P−O bond) associated with hydroxyapatite. A ($v1$) carbonate ($(CO_3)^{2-}$) A-ion type

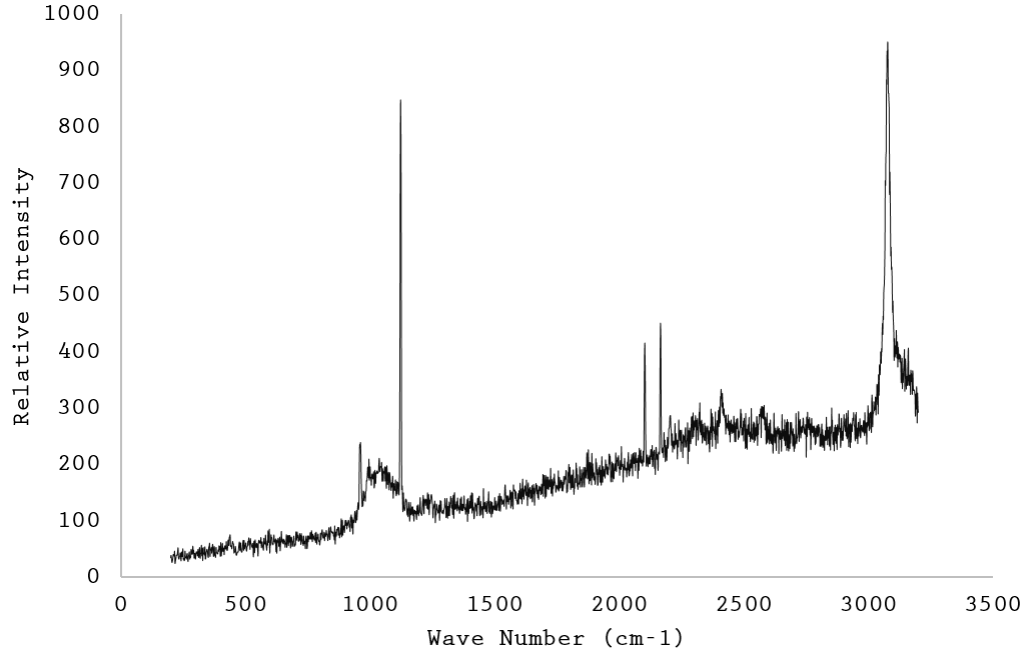

Fig. 5. Raman spectrum of untreated calcined cow bones.

substitution with a C-O planar valence was observed at 1123.53cm^{-1} which points to the presence of carbonate inclusions precipitating together with phosphates within the crystal lattice of hydroxyapatite. There were no peaks within the amide regions representing Amide III groups (region 1210 cm^{-1} - 1289 cm^{-1}), Amide II (1515 cm^{-1} - 1565 cm^{-1}) and Amide I (1625 cm^{-1} - 1675 cm^{-1}), respectively, this confirms that the calcination process eliminated the collagen content of the cow bones [28]. The harmonic overtone or combination bands at 2103.70 cm^{-1} and 2166.38 cm^{-1} indicate alkyne and hydroxyl groups which are overlapped with the frequencies of bound water. The peak at 2622.93 cm^{-1} band is due to symmetric stretching vibration of the aliphatic CH_2, and the CH stretching band at 3076.87 cm^{-1} indicates the presence of other organic phases apart from collagen within the cow bone sample.

Scanning electron microscopy with energy dispersive spectroscopy (SEM - EDS)

The morphology of the calcined CB sample is shown in Fig. 6 and the EDS is shown in Fig. 7. The SEM photomicrograph shows large lumps with a porous sponge-like structure surrounded by numerous tiny spikes jutting out of the surface of each lump in a random manner. This morphology is likely due to high temperature sintering of micro particles of calcium based bones during calcination at 1000°C into small spikes, which in turn agglomerate into larger lumps. These large lumps are also characterised by a porous structure as the organic materials within the bones are burnt off. These numerous pores are clearly visible on the lumps with tiny spikes noticeably attached to each surface resulting in a corresponding variation in particle size.

The particles were all randomly dispersed and well distributed with an average particle size of 7.4 μm, derived from the SEM micrograph as illustrated by the histogram in Fig. 8. The white phases are the cow bone derived hydroxyapatite particles and other calcium phosphate compounds. This is revealed by the EDS spectrum and semi-quantitative analysis data obtained and shown in Fig. 7. This data reveals the elemental composition of the calcined powders and identifies the major sharp peaks in the spectrum as 43.29 wt. % calcium, 39.36 wt. % oxygen, and 16.31 wt. % P, while minor peaks of magnesium and aluminium were identified in trace amounts of 0.57 wt. % and 0.46 wt. %, respectively. This, therefore, confirms that stoichiometric hydroxyapatite composed mainly of calcium and phosphorus with a Ca/P mole ratio of 1.67 was derived from the calcined untreated cow bone samples, which is in agreement with the XRD results.

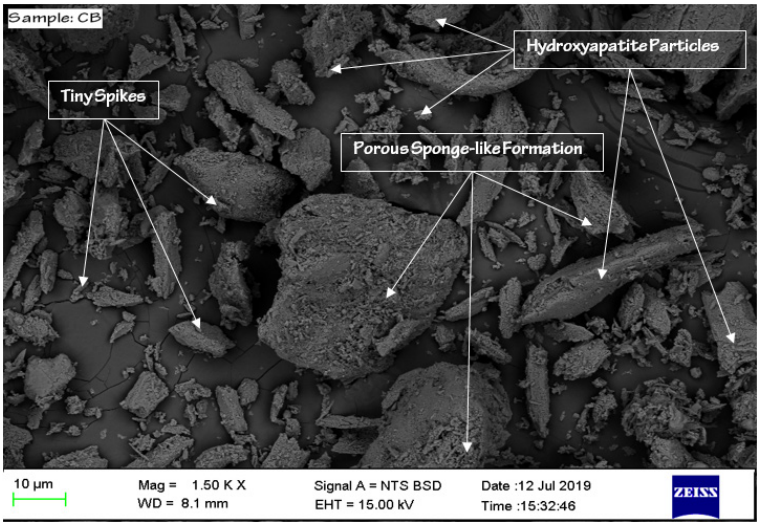

Fig. 6. SEM micrograph of the untreated calcined cow bone powders.

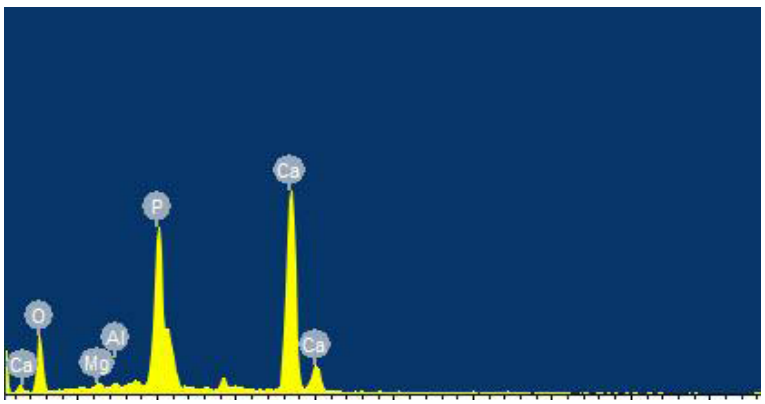

Fig. 7. EDS spectrum and data of the untreated calcined cow bone powders.

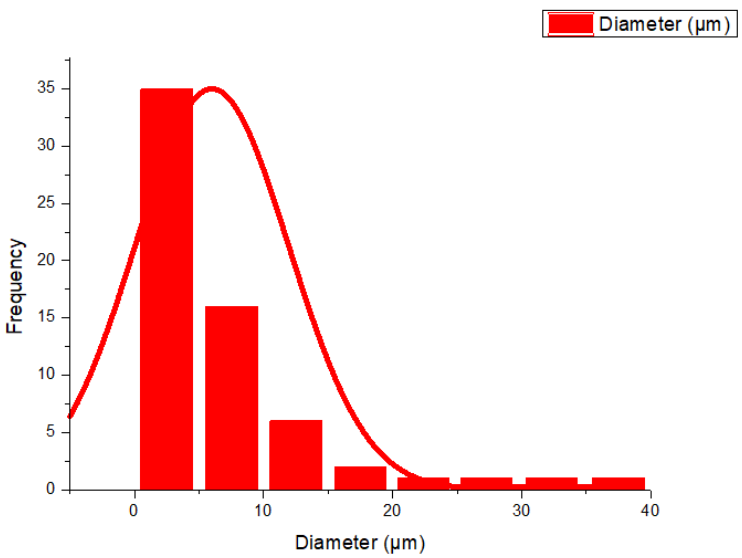

Fig. 8. Histogram showing the average particle size of the untreated calcined cow bone powders.

CONCLUSIONS

Analysis of the results for the determination of the most suitable process for the synthesis of hydroxyapatite from natural sources has been successfully carried out. Hydroxyapatite obtained by calcination was found to be superior to those derived by both wet chemical precipitation methods. It was discovered that the sample contained a wider variety of elements compared to others with a porous structure and a Ca/P ratio of 1.67, which made it the most structurally compatible when compared to human bone. The structural morphology of the resultant hydroxyapatite compounds revealed a porous sponge-like spiky structure which indicated the level of agglomeration, ease of blood flow, cell proliferation and adhesion. Hence, the results revealed that cow bones do not need to be subjected to chemical synthesis but calcination in order to obtain quality HAp for use in the development of implants.

REFERENCES

1. F. Morgan, G.L. Barnes, T.A. Einhorn, In: Osteoporosis. R. Marcus, D. Feldman, D.A. Nelson, C.J., Rosen (Eds), Academic Press, San Diego, 2008, 3-26.
2. W. Zhu, P.G. Robey, A.L. Boskey, In: Osteoporosis. R. Marcus, D. Feldman, D.A. Nelson, C.J., Rosen (Eds), Academic Press, San Diego, 2008, 191-240.
3. A.K. Teotia, D.B. Raina, C. Singh, N. Sinha, H. Isaksson, M. Tägil, L. Lidgren, A. Kumar, Nano-Hydroxyapatite Bone Substitute Functionalized with Bone Active Molecules for Enhanced Cranial Bone Regeneration, ACS Appl. Mater. Interfaces. 9, 8, 2017, 6816-6828.
4. S.M. Zakaria, S.H. Sharif Zein, M.R. Othman, F. Yang, J.A. Jansen, Nanophase hydroxyapatite as a biomaterial in advanced hard tissue engineering: a review, Tissue Eng Part B Rev., 19, 5, 2013, 431-41.
5. C.H. Cik-Rohaida, B. Idris, Y. Mohd Reusmaazran, M. Rusnah, A.M. Fadzley Izwan, Hydroxapatite tricalcium phosphate prepared by precipitation method, Med. J. Malaysia, 59, 2004, 156-7.
6. I.O. Oladele, O.G. Agbabiaka, O.G. Olasunkanmi, A.O. Balogun, M.O. Popoola, Non-synthetic sources for the development of hydroxyapatite, Journal of Applied Biotechnology & Bioengineering, 5, 2, 2018a, 88-95.
7. O.G. Agbabiaka, I.O. Oladele, A.D. Akinwekomi, A.A. Adediran, A.O. Balogun, O.G Olasunkanmi T.M.A. Olayanju, Effect of calcination temperature on hydroxyapatite developed from waste poultry eggshell, Scientific Africa, 8, 2020, 1-12.
8. S.A.S. Bonou, E. Sagbo, C. Aubry, C. Charvillat, B. Ben-Nissan, S. Cazalbou, Conversion of Snail Shells (*Achatina achatina*) Acclimatized in Benin to calcium Phosphate for Medical Engineering Use, Journal of the Australian Ceramic Society, 55, 2019, 1177-1186.
9. P. Hui, S.L. Meena, G. Singh, R.D. Agarawal, S. Prakash, Synthesis of hydroxyapatite bio-ceramic powder by hydrothermal method, J. Miner. Mater. Charact. Eng., 09, 2010, 683-692.
10. I.O. Oladele O.S. Akinola O.G. Agbabiaka J.A. Omotoyinbo, Mathematical Model for the Prediction of Impact Energy of Organic Material Based Hydroxyapatite (HAp) Reinforced Epoxy Composites, Fibers Polymers, 19, 2, 2018b, 452-459.
11. S. Rujitanapanich, P. Kumpapan, P. Wanjanoi, Synthesis of Hydroxyapatite from Oyster Shell via Precipitation, Energy Procedia, 56, 2014, 112 - 117.
12. M. Akram, R. Ahmed, I. Shakir, Extracting Hydroxyapatite its Precursors from Natural Resources, Journal of Materials Science, 49, 4, 2014, 1461-1475.
13. N.A.M. Barakat, M.S. Khil, A.M. Omran, F.A. Sheikh, H.Y. Kim, Extraction of pure natural hydroxyapatite from the bovine bones bio waste by three different methods, J Mater Process Tech, 209, 2009, 3408-3415.
14. O. Borkiewicz, J. Rakovan, C.L. Cahill, Time-resolved in situ studies of apatite formation in aqueous solutions, Am Mineral, 95, 8-9, 2010, 1224-1236.
15. J. C. Elliott Structure chemistry of the apatites other calcium orthophosphates, Elsevier Amsterdam, 1994, 4.
16. K. YoungJae, L. Seon Yong, R. Yul, L. Jinhyeok, K. Juyeun, L. Yongwoo, B. Junseok, L. Young Jae, Optimizing calcium phosphates by the control of pH temperature via wet precipitation, J Nanosci Nanotechnol., 15, 2015, 10008-10016.
17. R.W. Marshall, G.H. Nancollas, The kinetics of crystal growth of dicalcium phosphate dehydrate,

J. Phys. Chem., 73, 11, 1969, 3838-3844.
18. G. Gergely, F. Wéber, I Lukács, A.L Tóth, Z.E Horváth, J. Mihály, C. Balázsi, Preparation characterization of hydroxyapatite from eggshell, Ceramics International, 36, 2, 2010, 803-806.
19. I.O. Oladele, O.G. Agbabiaka, A.A. Adediran, A.D. Akinwekomi, A.O. Balogun, Structural performance of poultry eggshell derived hydroxyapatite based high density polyethylene bio-composites, Heliyon, 5, 2019, 1-17.
20. O. Mekmene, S. Quillard, T. Rouillon, J.M. Bouler, M. Piot, F. Gaucheron, Effects of pH Ca/P molar ratio on the quantity crystalline structure of calcium phosphates obtained from aqueous solutions, Dairy Science & Technology EDP, sciences/ Springer, 89, 3-4, 2009, 301-316.
21. J. Duncan, J.F. MacDonald, J.V. Hanna, Y. Shirosaki, S. Hayakawa, A. Osaka, J.M.S. Skakle, I.R. Gibson, The role of the chemical composition of monetite on the synthesis properties of β- tricalcium phosphate, Mater Sci Eng, 34, 2014, 123-129.
22. S. Mondal, B. Mondal, A. Dey, S.S Mukhopadhyay, Studies on processing characterization of hydroxyapatite biomaterials from different bio wastes, J. Miner. Mater. Characterization Eng., 2012, 11, 55-67.
23. L. Berzina-Cimdina, N. Borodajenko, Research of calcium phosphates using fourier transform infrared spectroscopy, Theophanides, T. ed. Infrared Spectroscopy-Materials Science, Engineering Technology, InTech, 2012, 123-148.
24. M. Igisu, Y. Ueno, K. Takai, FTIR microspectroscopy of carbonaceous matter in ~3.5 Ga seafloor hydrothermal deposits in the North Pole area, Western Australia, Progress in Earth Planetary Science, 5, 2018, 85.
25. R.A Bakar, R. Yahya, S.N. Gan, Production of High Purity Amorphous Silica from Rice Husk, Procedia Chemistry, 19, 2016, 189-195.
26. S.V Ganachari, A.A Bevinakatti, J.S Yaradoddi, N.R Banapurmath, A.M Hunashyal, A.S Shettar, Rapid synthesis, characterization, studies of hydroxyapatite nanoparticles, Adv Mater Sci Res, 1, 1, 2016, 9-13.
27. B.O Fowler, M. Markovic´, W.E Brown, Octacalcium phosphate carboxylates. 3. Infrared Raman vibrational spectra, Chem Mater, 5, 1993, 1417-1423.
28. C.P Tarnowski, M.A Ignelzi, Jr, M.D Morris, Mineralization of Developing Mouse Calvaria as Revealed by Raman Microspectroscopy, Journal of Bone Mineral Research, 17, 6, 2002, 1118-1126.